Polymer-templated nucleation and crystal growth of perovskite films for solar cells with efficiency > 21%

Dongqin Bi,[1] Chenyi Yi,[2] Jingshan Luo,[2] Jean-David Décoppet,[2] Fei Zhang,[2] Shaik Mohammed Zakeeruddin,[2] Xiong Li,[2] Michael Grätzel[2]* & Anders Hagfeldt[1]*

[1]Laboratory of Photomolecular Science, Ecole polytechnique fédérale de Lausanne, CH-1015 Lausanne, Switzerland.

[2]Laboratory of Photonics and Interfaces, Ecole polytechnique fédérale de Lausanne, CH-1015 Lausanne, Switzerland.

*Corresponding author. Email: michael.graetzel@epfl.ch and anders.hagfeldt@epfl.ch

The past several years have witnessed the rapid emergence of a new class of solar cells based on mixed organic-inorganic halide perovskites. Today's state of the art pervoskite solar cells (PSCs) cells employ various methods to enhance nucleation and improve the smoothness of the perovskite films formed via solution processing. However, the lack of precise control over the crystallization process creates a risk of forming unwanted defects, e.g. pin holes and grain boundaries. Here, we introduce a new approach to prepare perovskite films of high electronic quality by using poly(methyl methacrylate) (PMMA) as a template to control nucleation and crystal growth. We obtain shiny smooth perovskite films of excellent electronic quality, as manifested by a remarkably long photoluminescence lifetime. We realize stable PSCs with excellent reproducibility showing an extraordinary power conversion efficiency (PCE) of up to 21.6% and a certified PCE of 21.02% under standard AM 1.5 reporting conditions.

Organic-inorganic halide perovskites are attractive materials for solar cells, because of their ease of fabrication, panchromatic absorption of sunlight and long carrier diffusion length[1]. Although the first solid-state perovskite cell with a power conversion efficiency (PCE) of 9.7% was reported only in 2012[2], the PCE was raised to over 20 % in 4 years (http://www.nrel.gov/ncpv/images/efficiency_chart.jpg). The control over both morphological and electronic properties of the perovskite films is crucial to achieve high-performance perovskite devices. Electronic trap states resulting from pinholes or crystal defects and grain boundaries enhance non-radiative recombination reducing severely the charge carrier lifetime and the photoluminescence (PL) yield. This in turn entails a loss in open-circuit voltage and overall conversion efficiency[3]. The morphology of solution-processed perovskite film is mainly governed by nucleation and crystal growth. Generally, inducing rapid nucleation and slowing down the crystal growth are promising ways to obtain perovskite films of high optoelectronic quality. A variety of methods have been developed to retard perovskite crystallization, such as adding HI or HCl acid[4-6], and employing additives like N,N-dimethyl sulfoxide (DMSO) or 1,8- diiodooctane (DIO) to form intermediate adducts with Pb^{2+} [7,8]. Several other techniques[9-12] have been developed to improve the nucleation process, among which antisolvent-dripping has turned out to be an efficient method [13,14] by triggering homogeneous nucleation at the surface of the formed layer (solid/antisolvent/air interfaces) to make smooth perovskite film with high surface coverage.[15] However, further exploration of enabling both faster nucleation and slower crystal growth remains challenging.

Here, we introduce polymer-templated nucleation and growth (PTNG) as a new method for crystal engineering of perovskites. The polymer [poly(methyl methacrylate), (PMMA)] enables heterogeneous nucleation which is believed to be

orders of magnitude faster than the homogeneous nucleation due to the lowering of the nucleation free energy barrier[16]. On the other hand, PMMA slows down the perovskite crystal growth by forming an intermediate adduct with PbI_2 to allow the randomly formed nuclei to adjust their orientation to minimize the total Gibbs free energy and grow in the thermodynamically preferred orientation[17]. The cooperation of these two effects results in smooth perovskite films with fewer defects and larger oriented grains, enabling us to fabricate perovskite solar cells with a PCE over 21%

Although PMMA has been widely used as a moisture protection barrier on top of the back contact of PSCs or mixed with carbon nanotubes to form the hole collection layer[18]. It has so far not been employed to affect the formation of the perovskite itself during solution processing. We produce the mixed cation perovskite films in a single step from a solution of formamidinium iodide (FAI), PbI_2, methylammonium bromide (MABr) and $PbBr_2$ in a mixed solvent of dimethyl formamide (DMF), dimethyl sulfoxide (DMSO) and N-methyl-2-pyrrolidone (NMP)[13]. During the spin-coating of the perovskite solution, we introduce PMMA in a chlorobenzene/toluene mixture to template crystal formation and growth of the perovskite. By using this technique for film deposition we fabricate perovskite solar cells with the structure Au/Spiro-OMeTAD/ perovskite /mesoporous TiO_2/compact TiO_2/FTO, the cross sectional scanning electron microscopy (SEM) image of which is shown in Fig. 1a. Employing this solar cell configuration, we achieve the best PCE of 21.6% with a PMMA concentration C_{PMMA} =0.6mg/ml. The photovoltaic metrics of the device are as follows: short-circuit current density (J_{SC}) = 23.7 mA cm^{-2}, open circuit voltage (V_{OC}) = 1.14 V, and a fill factor (FF) = 0.78 (Fig. 1b). One of the devices was sent for certification to Newport Corporation PV Lab, an accredited PV testing laboratory, confirming a PCE of 21.02% (supplementary Fig.1). The

commonly observed hysteresis[19] is virtually negligible in our devices as proven by *J-V* curves shown in Fig. 1b. A histogram of two batches of cells (supplementary Fig. 2, Tab.1) indicates excellent reproducibility with an average PCE of 21.0%. Preliminary stability investigations show that the unsealed devices containing PMMA are stable showing only a 3.3% decay in PCE during exposure to ambient air for two months in the dark (supplementary Fig. 3, Tab. 2a and 2b). The photovoltaic metrics of the PSCs fabricated from PTNG method varying C_{PMMA} are summarized in Fig. 1c. Upon increasing the PMMA concentrations (C_{PMMA}, mg/ml) in mixed chlorobenzene and toluene (volume ratio of cholorobenzene and toluene is 9:1) solution, the PCE first augments and subsequently decreases with a peak at C_{PMMA} = 0.6. Upon increasing the C_{PMMA} from 0 to 0.6 mg/ml, the V_{oc} rises from 1.10V to 1.14 V, and the FF from 0.74 to 0.78.

Fig. 2 shows the scanning electron microscopy (SEM) images of perovskite films deposited on m-TiO$_2$/c-TiO$_2$/FTO substrate by varying C_{PMMA}. As illustrated by the left column of images the morphology of the pre-perovskite intermediates[20] present before annealing, changes from a mixture of randomly-distributed nanoparticles into homogeneous nanorods. The middle and right columns of images show the perovskite film after annealing, the grain size of the perovskite film produced by PTNG method increases with the C_{PMMA} and most of the grain boundaries become perpendicular to the substrate, benefitting reducing surface area of grain boundaries. Hence, the PMMA is expected to uniformly trigger heterogeneous nucleation over the perovskite precursor film, improving the grain size and facilitating the perovskite to grow in preferred direction reflection of facet with (111) indices being dominant because of the low symmetry of the trigonal perovskite (p3m1) phase as indicated in the XRD pattern in Fig. 3a.. Whereas numerous grain boundaries exist

in cross-sectional SEM of the reference film, no obvious boundary exists in the PTNG treated film. On the other hand, above $C_{PMMA} > 0.6$ mg/ml, new species appeared on the surface of perovskite grains, which we attribute to PMMA particles as the brighter signal indicate charge accumulation resulting from poor conductivity. This phenomenon accounts for the deterioration of the PV metrics when C_{PMMA} exceeds 0.6 mg/ml PMMA because of the excess of PMMA will impair charge carrier collection.

To further examine the crystal structure, we conducted thin layer X-ray diffraction (XRD) measurements for perovskite films deposited on m-TiO$_2$/bl-TiO$_2$/FTO substrates (Fig.3a). The peak at 12.5^o arises from the (001) lattice planes of hexagonal (2H polytype) PbI$_2$. The excess PbI$_2$ is believed to passivate surface defects, increasing the solar cell performance[13]. All the samples show the same trigonal perovskite phase with the dominant (111) lattice reflection. We speculate the (111) plane to exhibit the smallest surface energy because the majority of grains exhibit this orientation to minimize the total Gibbs free energy of the system. With increasing C_{PMMA}, the (111) oriented grains grew faster by consuming neighboring non-oriented crystals, either by regular grain growth or grain attachment, as evidenced by the increased ratio between the (111) and (123) peak at 13.9 ° and 31.5° in the presence of PMMA. By taking the full width at half maximum (FWHM) of the (111) reflection, we calculate the crystallite size using Scherrer's equation. Their dimension increases from 41 to 55, 70, 94, and 112 nm by increasing C_{PMMA} from 0 to 4mg/ml. We attribute the larger crystal sizes to the templating effect of PMMA on the crystal growth. The carbonyl groups in PMMA form an intermediate adduct with PbI$_2$ as revealed by the Fourier transform infrared spectroscopy (FTIR) spectra in Fig. 3b. The stretching vibration of C=O bond in pure PMMA appears at 1735 cm^{-1}, while it

shifted to 1723 cm^{-1} upon interaction with PbI$_2$. The shift of the C=O vibration in PMMA to higher wavenumber upon interaction with PbI$_2$ is indicative of formation of an intermediate PMMA-PbI$_2$ adduct, since it is a consequence of a weakened C=O bond strength caused by interaction with the Lewis acid PbI$_2$. The formation of such an adduct[7] is expected to retard the crystal growth and improve the crystallity of the perovskite film.

To analyze the dynamics of recombination, we performed time resolved photoluminescence (TRPL) decay measurements. (Supplementary Fig.4,5)The PL decays for perovskite films with C_{PMMA}=0 and 0.6mg/ml deposited on a m-TiO$_2$/c-TiO$_2$/FTO substrate are shown in Fig. 3c, revealing a much faster PL decay for the reference than the PMMA-treated film. The PL decay curves were fitted to a bi-exponential rate law:

$$Y=A_1*\exp(-t/\tau_1) + A_2*\exp(-t/\tau_2) + y_0,$$

where A$_1$ and A$_2$ are relative amplitudes, while τ_1 and τ_2, are lifetimes for the fast and slow recombination, respectively[21]. The decay is attributed mainly to trap-assisted recombination at defects. The film with the PMMA treatment shows for the fast and slow phase lifetimes of τ_1=23.9 ns (fraction A$_1$=0.37) and τ_2=259.3 ns, (fraction A$_2$=0.63), respectively. By contrast, the sample without the PMMA treatment gives τ_1=18.7 ns (fraction A$_1$=0.66) and τ_2=123.6 ns, (fraction A$_2$=0.34), respectively. This indicates a lower defect concentration and hence superior electronic quality for the PMMA-containing perovskite polycrystalline film, consistent with the higher Voc of the corresponding PSC[13].

The X-ray photoelectron spectroscopy (XPS) in Fig. 3d shows Pb 4f spectra. There are two main peaks Pb 4f7/2 and Pb 4f5/2 at 138 and 142.8 eV, respectively. We attribute the two small peaks located at 136.4 and 141.3 eV to the presence of

metallic Pb[22].The presence of a substantial amount of atomic Pb is an indication of the existence of iodide vacancies in the perovskite lattice of the control sample. The metallic lead species in the film are likely to act as non-radiative recombination centers which impairs solar cell operation. Thus, elimination of the metallic lead content is critical to realize perovskite films of better electronic quality[21] Interestingly, the atomic Pb peak is greatly reduced in the PMMA treated films, probably due to a lower level of iodide vacancies in the crystal lattice of the PMMA treatment films. A lower level of Pb defects can reduce the non-radiative recombination and increase the PL lifetime, in line with the TRPL results.

In conclusion, we introduce a new method for preparing high-electronic quality perovskite films and implement it for the fabrication of PSC with excellent performance their certified PCE attaining 21 %. Further development of the method will enable further performance gains.

author(s) and do not necessarily reflect the official opinion of the European Union. Neither the European Union institutions and bodies nor any person acting on their behalf may be held responsible for the use that which may be made of the information contained herein.

Author contribution: D.B. conceived and carried out the experimental study on device fabrication and basic characterization including photovoltaic measurement and XRD and wrote the manuscript together with M.G.,X.L. and Y.C. Y.C. did help for PL and XPS measurement. F.Z. provided TiO_2 film. L.J. did the SEM measurement. J.D and S.M.Z. did help for the certification. X.L. assisted in fabricating the device and preparing the manuscript. A.H. and M.G. supervised the project. Competing interests: The authors declare that they have no competing interests. Data and materials availability: All data needed to evaluate the conclusions in the paper are present in the paper and/or in the Supplementary Materials. Additional data are available from D.B. (dongqin.bi@epfl.ch) upon request.

References

1. G. Hodes, Perovskite-Based Solar Cells. *Sci.* **342**, 317–318 (2013).

2. Kim, H.S. et al. Lead Iodide Perovskite Sensitized All-Solid-State Submicron Thin Film Mesoscopic Solar Cell with Efficiency Exceeding 9%. *Sci. Rep.* **2**, 591 (2012).

3. Nie, W. et al. High-efficiency solution-processed perovskite solar cells with millimeter-scale grains. *Sci.* **347**, 522-525 (2015).

4. Li, G., Zhang, T. & Zhao, Y. Hydrochloric acid accelerated formation of planar $CH_3NH_3PbI_3$ perovskite with high humidity tolerance. *J. Mater. Chem. A* **3**, 19674-19678 (2015).

5. Eperon, G.E. et al. Formamidinium lead trihalide: a broadly tunable perovskite for efficient planar heterojunction solar cells. *Energy & Environ. Sci.* **7**, 982-988 (2014).

6. Yang, L., Wang, J. & Leung, W.W.F. Lead Iodide Thin Film Crystallization Control for High-Performance and Stable Solution-Processed Perovskite Solar Cells. *ACS Appl. Mater. & Inter.* **7**, 14614-14619 (2015).

7. Lee, J.-W., Kim, H.S. & Park, N.-G. Lewis Acid–Base Adduct Approach for High Efficiency Perovskite Solar Cells. *Acc. Chem. Res.* **49**, 311-319 (2016).

8. Liang, P.-W. et al. Additive Enhanced Crystallization of Solution-Processed Perovskite for Highly Efficient Planar-Heterojunction Solar Cells. *Adv. Mater.* **26**, 3748-3754 (2014).

9. Huang, F. et al. Gas-assisted preparation of lead iodide perovskite films consisting of a monolayer of single crystalline grains for high efficiency planar solar cells. *Nano Energy* **10**, 10-18 (2014).

10. Jeon, N.J. et al. Solvent engineering for high-performance inorganic–organic hybrid perovskite solar cells. *Nat. Mater.* **13**, 897-903 (2014).

11. Tidhar, Y. et al. Crystallization of Methyl Ammonium Lead Halide Perovskites: Implications for Photovoltaic Applications. *J. Am. Chem. Soc.* **136**, 13249-13256 (2014).

12. Bi, C. et al. Non-wetting surface-driven high-aspect-ratio crystalline grain growth for efficient hybrid perovskite solar cells. *Nat.Commun.* **6**,7747 (2015).

13. Bi. D., *et al.*, Efficient luminescent solar cells based on tailored mixed-cation perovskites. *Sci. Adv.* **2**, 1501170 (2016)

14. Green, M. A.; Emery, K.; Hishikawa, Y.; Warta, W.; Dunlop, E. D., Solar cell efficiency tables (version 47). Prog. Photovolt: Res. Appl. **24**, 3-11 (2016)

15. Minemawari, H.; Yamada, T.; Matsui, H.; Tsutsumi, J. y.; Haas, S.; Chiba, R.; Kumai, R.; Hasegawa, T., Inkjet printing of single-crystal films. Nat. **475**, 364-367 (2011).

16. Cacciuto, A., Auer, S. & Frenkel, D. Onset of heterogeneous crystal nucleation in colloidal suspensions. *Nat.* **428**, 404-406 (2004).

17. S. Auer, D. Frenkel, Suppression of crystal nucleation in polydisperse colloids due to increase of the surface free energy. *Nat.* **413**, 711–713 (2001).

18. Habisreutinger, S.N. et al. Carbon Nanotube/Polymer Composites as a Highly Stable Hole Collection Layer in Perovskite Solar Cells. *Nano. Lett.* **14**, 5561-5568 (2014).

19. Shao, Y., Xiao, Z., Bi, C., Yuan, Y. & Huang, J. Origin and elimination of photocurrent hysteresis by fullerene passivation in $CH_3NH_3PbI_3$ planar heterojunction solar cells. *Nat. Commun.* **5**, 5784 (2014).

20. Guo, Y. et al. Chemical Pathways Connecting Lead(II) Iodide and Perovskite via Polymeric Plumbate(II) Fiber. *J. Am. Chem. Soc.* **137**, 15907-15914 (2015).

21. Cho, H. et al. Overcoming the electroluminescence efficiency limitations of perovskite light-emitting diodes. *Sci.* **350**, 1222-1225 (2015).

22. Lindblad, R. et al. Electronic Structure of TiO_2/$CH_3NH_3PbI_3$ Perovskite Solar Cell Interfaces. *J. Phys. Chem. Lett.* **5**, 648-653 (2014).
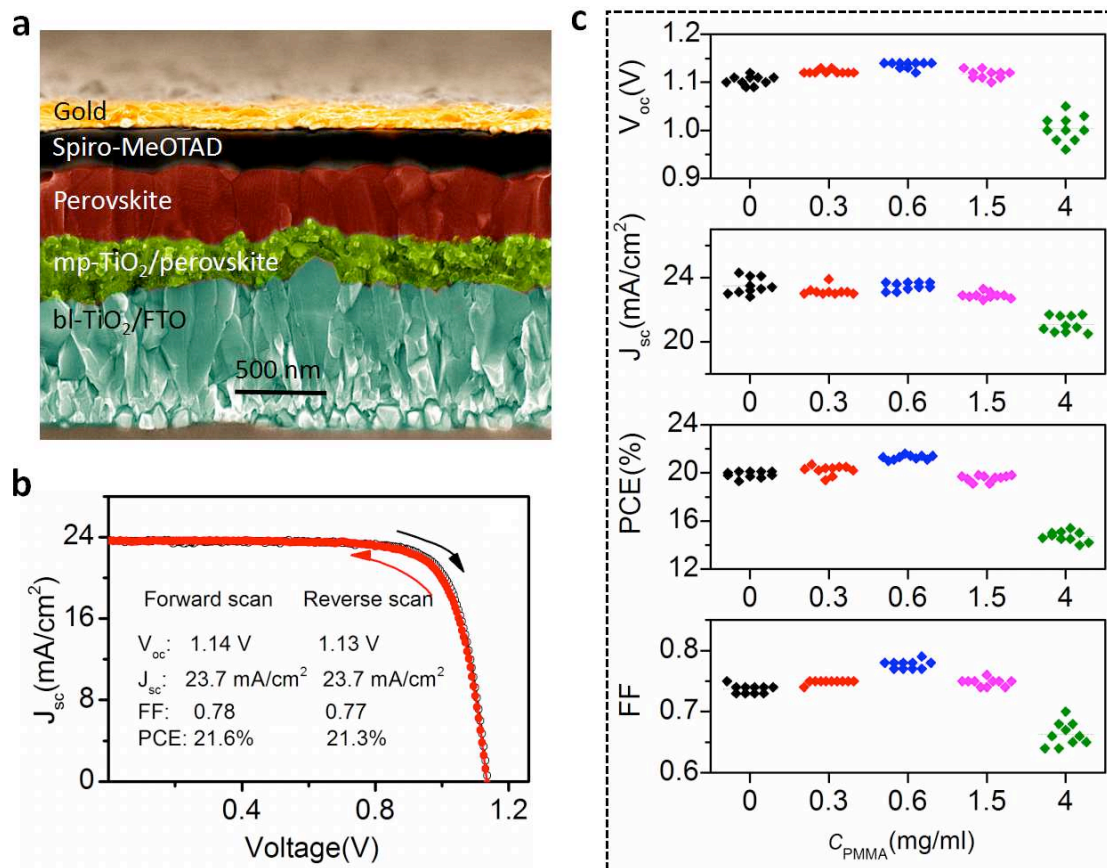
Fig.1 Device structure and performance. (a) A high-resolution cross section SEM image of a complete solar cell fabricated by PTNG method, where a smooth and compact perovskite capping layer fully covers the mesoporous TiO_2 layer (mp-TiO_2) infiltrated with perovskite. FTO, fluorine-doped tin oxide; bl-TiO_2, TiO_2 compact layer. **(b)** J-V curves of the champion PSC prepared by the PTNG method measured in both reverse and forward direction. **(c)** Photovoltaic metrics of devices plotted as a function of PMMA concentrations (C_{PMMA}, mg/ml) in mixed chlorobenzene and toluene (volume ratio of cholorobenzene and toluene is 9:1) solution.
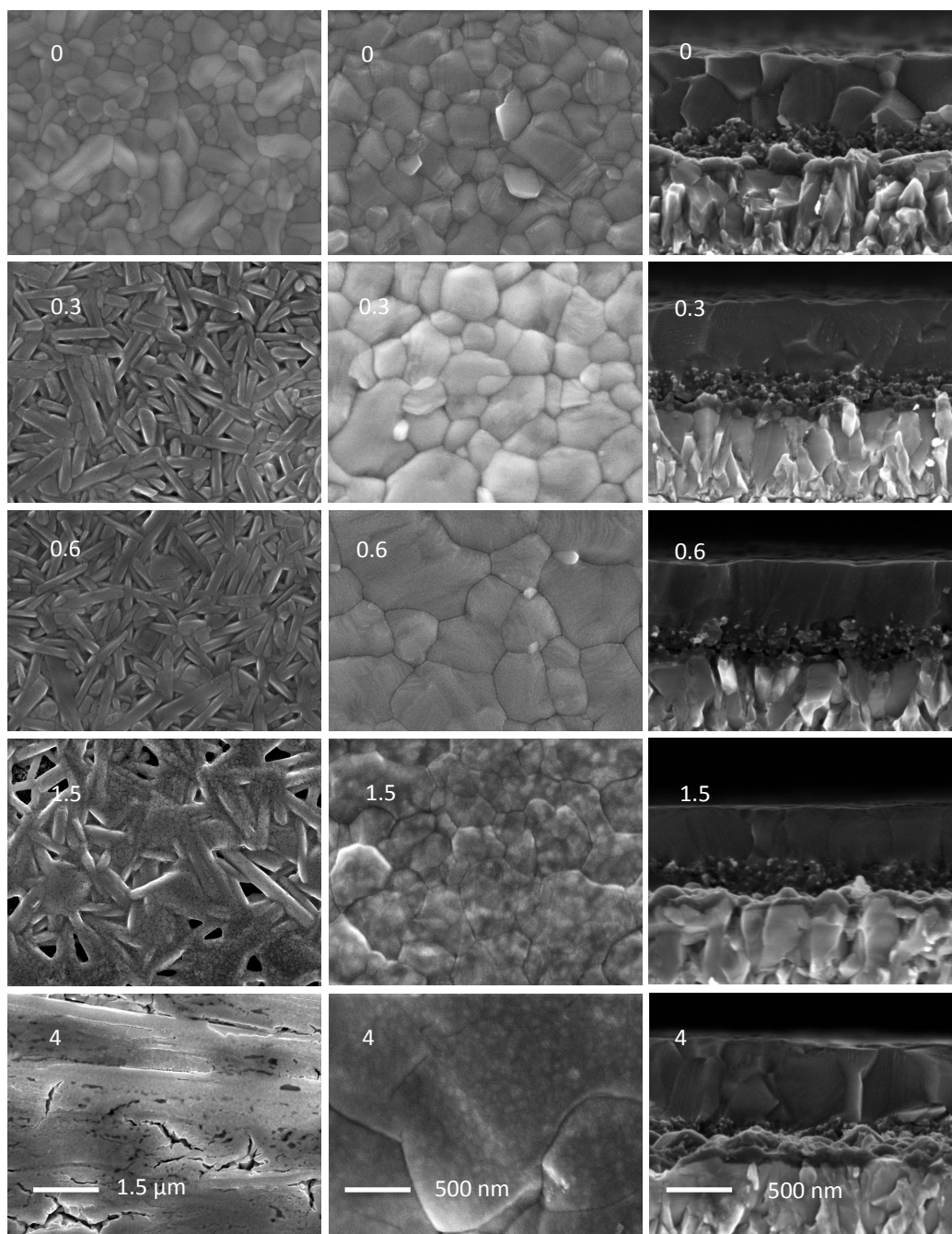
Fig.2. Scanning electron microscopic images. Top (left and middle colum) and cross sectional (right column) SEM of perovskite films deposited by PTNG method with different concentrations (mg/ml) of PMMA. The left column of images are perovskite film before annealing, while the middle ones and the right ones are films after annealing.
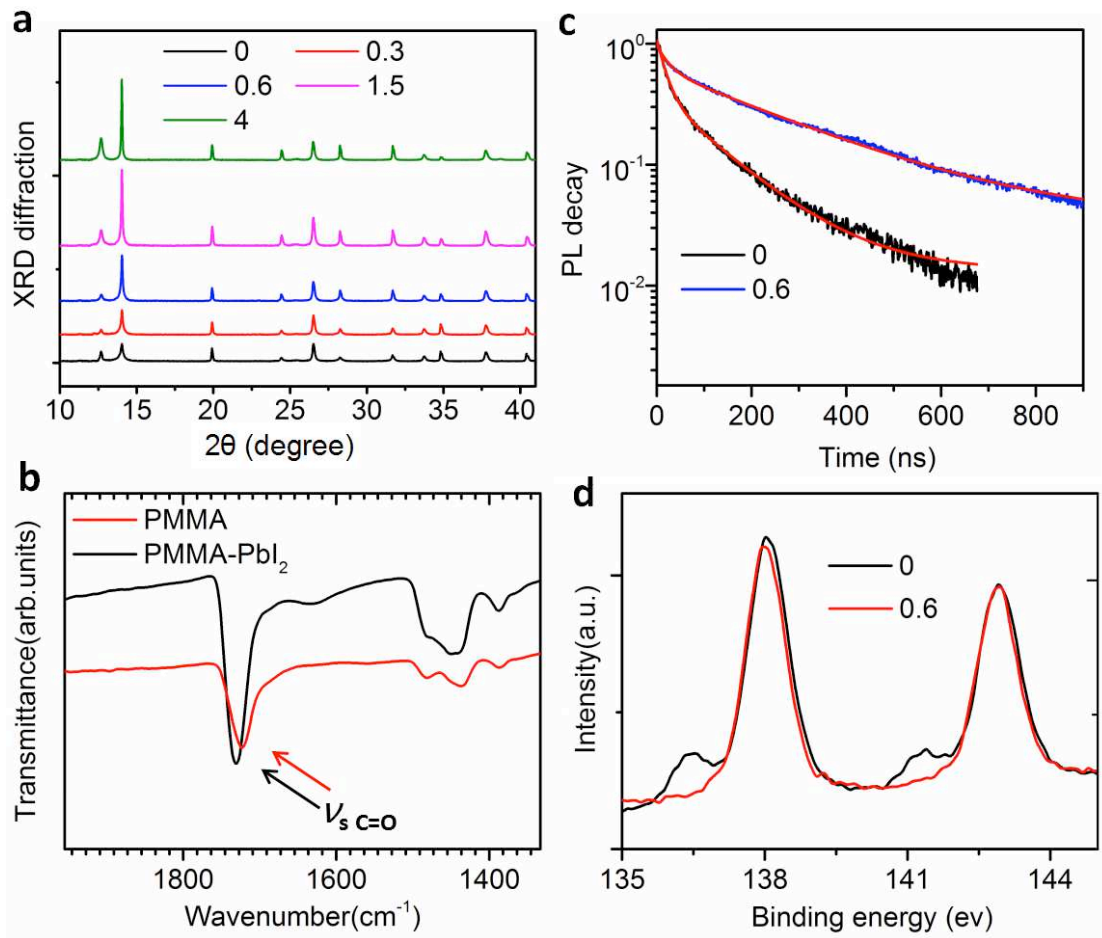
Fig. 3. Comparison of the XRD patterns, FTIR spectra, time resolved photoluminescence (PL) measurements (TRPL) and X-ray photonelectron spectrocopy (XPS) spectra for perovskite or PbI$_2$ films containing different content of PMMA. (a) XRD patterns of perovskite film using different concentration of PMMA solution. **(b)** FTIR spectra of PbI$_2$·PMMA prepared by mixing PMMA with PbI$_2$ in a molar ratio of 1:1. **(c)** TRPL and **(d)** XPS of perovskite film treated by PTNG method with different PMMA concentrations.